

All you ever wanted to know about optical long baseline stellar interferometry, but were too shy to ask your adviser

Florentin Millour ^a

^a*Max-Planck Institute Für Radio-astronomie, Auf dem Hügel 69, 53121 Bonn, Germany*

Abstract

I try to present a small view of the properties and issues related to astronomical interferometry observations. I recall a bit of history of the technique, give some basic assessments to the principle of interferometry, and finally, describe physical processes and limitations that affect optical long baseline interferometry and which are, in general, very useful for everyday work. Therefore, this text is not intended to perform strong demonstrations and show accurate results, but rather to transmit the general “feeling” one needs to have to not be destabilised by the first contact to real world interferometry.

Key words: Optical long baseline interferometry, Visibility, Phase, UV coverage, VLTI, Keck-I

1 What is optical / IR long baseline interferometry ?

1.1 In the beginning ...

The discovery of the wave-property of light was probably made by Young (1800), who managed to produce light interferences by letting it go through 2 close holes. Soon after this discovery, Fizeau (1851) proposed and Stephan (1874) tried unsuccessfully to use this wave-property of light to measure the apparent diameter of stars at the *Observatoire de Marseille* with a 80 cm telescope.

Then, Michelson and Pease (1921) managed to measure the diameter of a star, Betelgeuse, equal to 0,047” with a relative accuracy of 10% using a larger interferometer (see Fig. 1, left) This experiment was very hard to carry out, the

first results (Pease , 1921a; Merrill , 1922) were so encouraging that a larger and more sensitive stellar interferometer (Pease , 1931) was built. However, technical drawbacks and mechanical instabilities were the major problems of these interferometers. Then, the project was abandoned during the second world war.

When the very first radio-telescopes put into operation, (Reber & Greenstein , 1947), the idea to coherently combine together several antennas was used to build radio-interferometers (Ryle , 1952). This enabled an increase in the spatial resolution of radio-collectors (Smith , 1952). An easy access to the measures allowed a swift progress of the instruments. This led to the VLA (Very Large Array, Butler et al. , 2006) and to the VLBA (Very Long Baselines Array, Cohen et al. , 1975).

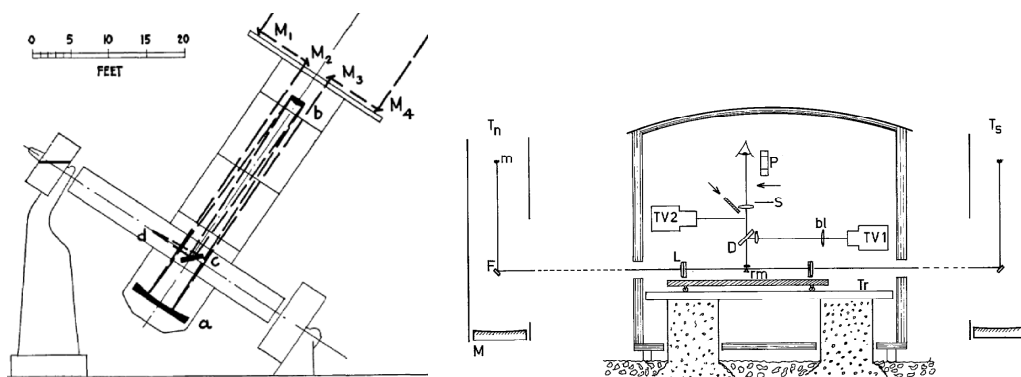


Fig. 1. **Left:** The *interferometer* of Michelson on the 100-inch telescope on the Mount Wilson (taken from reference Michelson and Pease , 1921). **Right:** The first Labeyrie (1975) interferometer (diagram is from the article).

1.2 Given up and reborn ...

In the optical domain, the techniques developed by Michelson were forgotten for more than 30 years. During this period, only intensity interferometry (Hanbury Brown & Twiss , 1956), which indirectly recombined the light, was developed and used for astronomy.

The true reborn of optical interferometry occurred in 1975 when A. Labeyrie (1975) managed to produce interference fringes on a star using two separate telescopes (see Fig. 1, right).

This achievement was repeated in numerous institutes where many prototypes

were built and then used for science (see Table 1). The initial concept was improved with the use of delay lines and stationary telescopes (Merkle , 1986) rather than moving optical tables and telescopes. The advent of *spatial filtering* (Coudé du Foresto et al. , 1997) and *simultaneous photometric calibration* allowed one to get rid of systematic effects (Perrin , 2003a,b). This enabled an advancement in accurate measurements.

Table 1

Working interferometers in the world in alphabetical order. NIR means *Near Infra-Red* (1-2.5 μ m) and MIR means *Mid Infra-Red* (8-13 μ m).

Name	Telescopes			Max. baseline	λ
	Diameter (m)	# Combined	Total		
CHARA	1	2	6	330	Visible, NIR
COAST	0.4	3	6	47	Visible, NIR
ISI	1.65	3	3	85	MIR
Keck-I	10	2	2	85	NIR, MIR
MIRA-I	0.25	2	2	30	Visible
NPOI	0.12	6	6	64	Visible
PTI	0.4	3	3	110	NIR
SUSI	0.14	2	2	640	Visible
VLTI	8 / 1.8	3 / 3	4 / 4	130 / 200	NIR, MIR

1.3 Interferometry today

Today’s interferometry follows two different tracks: larger baselines to get higher angular resolutions and larger telescope diameters to reach higher magnitudes. The Keck-I and the VLTI, which combines both large baselines and large apertures, are leading the way.

Keck-I: The Keck-I is a US project consisting of two very large 10 m segmented telescopes separated by 85 m. The Keck telescopes work in two main modes: independently or combined in the interferometric mode. This last mode uses two instruments: a coaxial re-combiner and a 2-telescope nuller. Today’s K-band limiting magnitude is 10, and it can work in low ($R \approx 20$) and medium

($R \approx 200$) spectral resolutions. A differential mode and a phase referencing mode are foreseen for the future. However, the initially planned additional small telescopes for the interferometers (the “outriggers”) have been abandoned, limiting the Keck-I project to a 2 telescope only interferometer.

VLTI: VLT (or *Very Large Telescope*) is European project mainly made of four 8 m telescopes (Unit Telescopes or UT) and a series of “small” 1.8 m telescopes (Auxiliary Telescopes or AT). Today, 4 ATs and 4 UTs are operational with baselines ranging from 16 m to 130 m (Fig. 2). Like the Keck telescope, the VLT can operate each 8 m telescope individually or combine up to three telescopes together using the VLTI or *Very Large Telescope Interferometer*. 3 instruments are now operational at VLTI:

VINCI: test instrument,

MIDI: mid-infrared instrument using 2 telescopes

AMBER: 3 telescope instrument in the near infrared.

Today’s VLTI is limited by vibrations, which are under investigation and should be solved in the next few years. The future of VLTI consists of a phase-referencing facility, PRIMA, and a series of projects for second-generation instruments (MATISSE, VSI, and GRAVITY).

1.4 Definitions

In this section, I will use the following notations:

- t is time,
- τ is delay,
- ω is the light pulsation and λ is its wavelength: $\omega = 2\pi C/\lambda$
- \vec{x} is the (x, y, z) coordinates vector,
- \vec{p} is the (x, y) coordinates vector in the pupil plane,
- \vec{s} is the (x, y) coordinates vector in the detector plane,
- \vec{u} is the (u, v) coordinates vector in the Fourier plane.

Other notations will be defined as they appear.

Electromagnetic wave: An electromagnetic wave ($\vec{E}(\vec{x}, t), \vec{B}(\vec{x}, t)$) is a particular case of an electric and magnetic field that propagates in space with

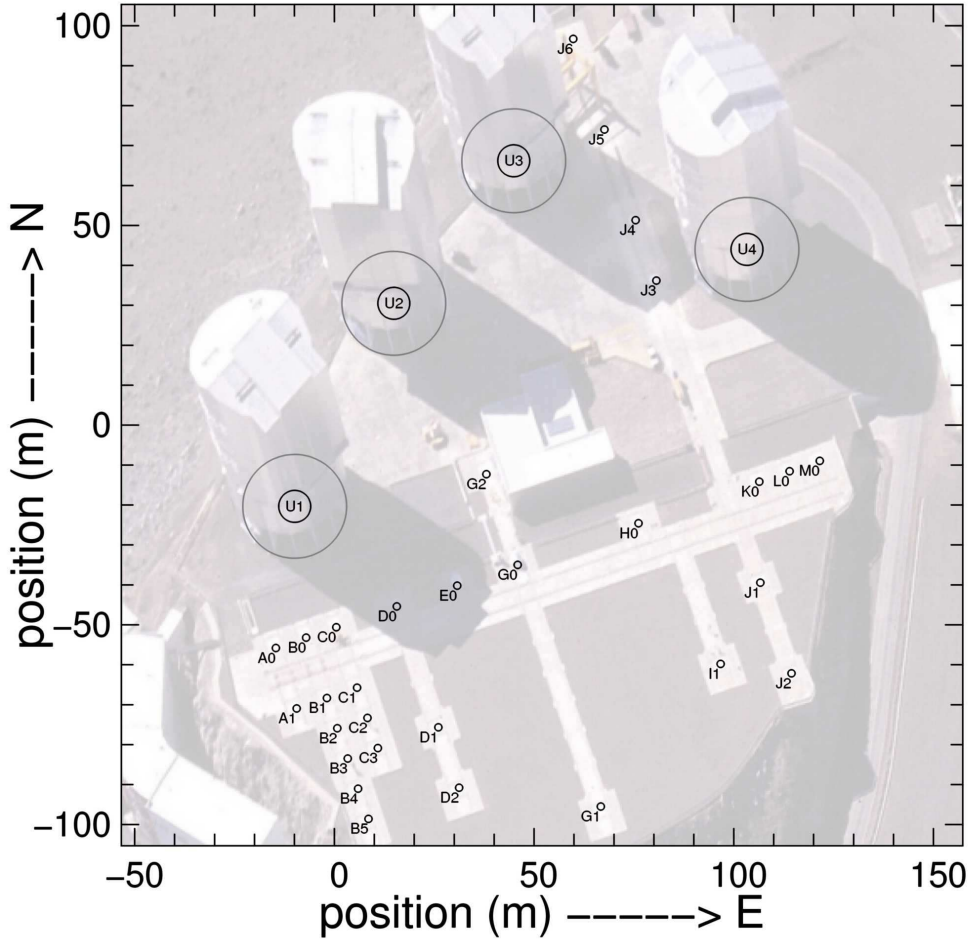


Fig. 2. Aerial view of the Paranal mountain and the Very Large Telescopes (photo credit: Gerhard Hüdepohl) under-plotted on the VLTI stations. Small stations correspond to ATs and larger encircled ones correspond to UTs.

time. The propagation of an electromagnetic wave is described by the Maxwell equations, and using the Lorentz gauge in space, it can take the following form:

$$\begin{aligned}\vec{E}(\vec{x}, t) &= \vec{E}_0(\vec{x})e^{i\omega t} \\ \vec{B}(\vec{x}, t) &= \vec{B}_0(\vec{x})e^{i\omega t}\end{aligned}\tag{1}$$

Light intensity: An optical or infrared detector is sensitive to the light intensity $I(\vec{s})$; i.e. the time-average of the squared modulus of the electromagnetic field at the measurement point:

$$I(\vec{s}) = \left\langle \|\vec{E}(\vec{s}, t)\|^2 \right\rangle_t\tag{2}$$

In this equation, \vec{s} are the spatial coordinates in the detector plane (see Fig. 3), t is the time, and \vec{E} is the electromagnetic field.

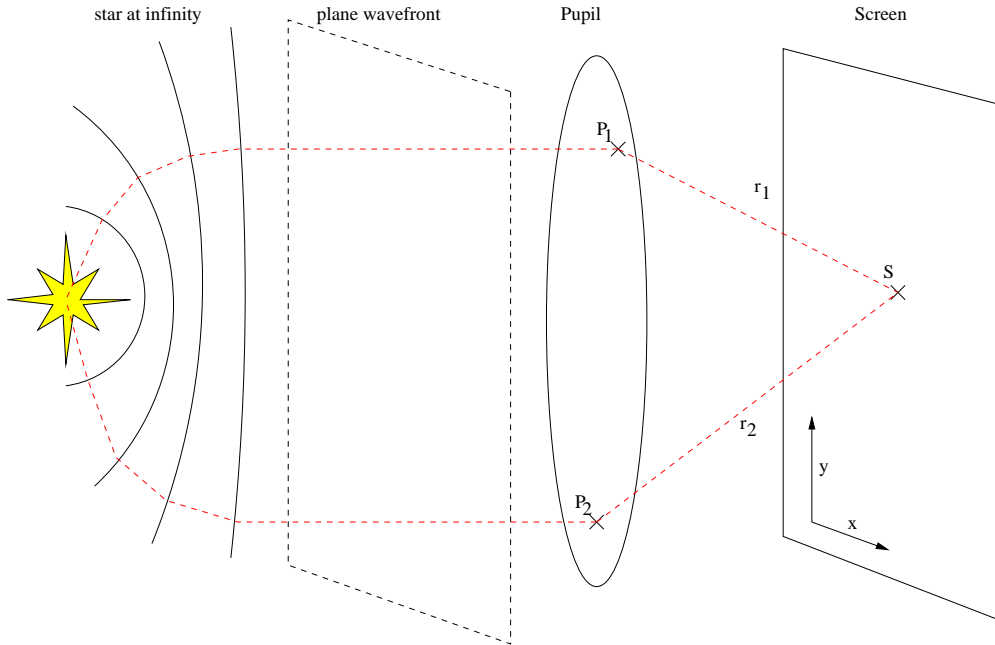


Fig. 3. The light propagation of an electromagnetic wave from a star at infinity to the detector plane (screen). Interferometry is interested in the study of the interaction between waves coming from two points of the initial wavefront. Notations come from the text.

1.5 What does an interferometer measure ?

Coherence between 2 waves: When observing an object with a given instrument, the light intensity I is the result of the superposition of many electromagnetic waves coming from different points of the instrument's pupil plane (see Fig. 3):

$$\begin{aligned}
 I(\vec{s}) &= \left\langle \left\| \vec{E}(\vec{s}, t) \right\|^2 \right\rangle_t \\
 &= \left\langle \left\| \sum_i \vec{E}(\vec{p}_i, t - \tau_i) \right\|^2 \right\rangle_t
 \end{aligned}
 \tag{3}$$

This expression applies when one is only interested in a 2-wave interaction:

$$I(\vec{s}) = \left\langle \left\| \vec{E}(\vec{p}_1, t - \tau_1) + \vec{E}(\vec{p}_2, t - \tau_2) \right\|^2 \right\rangle_t \quad (4)$$

If one defines the mutual coherence function $\Gamma_{1,2}$ by:

$$\Gamma_{1,2}(\tau) = \left\langle \vec{E}(\vec{p}_1, t - \tau) \vec{E}^*(\vec{p}_2, t) \right\rangle_t \quad (5)$$

The light intensity can be expressed in a simple way:

$$I(\vec{s}) = \Gamma_{1,1}(0) + \Gamma_{2,2}(0) + \Gamma_{1,2}(\tau_2 - \tau_1) + \Gamma_{1,2}^*(\tau_2 - \tau_1) \quad (6)$$

Then one can define the complex coherence degree $\gamma_{1,2}(\tau)$ as:

$$\gamma_{1,2}(\tau) = \frac{\Gamma_{1,2}(\tau)}{\Gamma_{1,1}(0) + \Gamma_{2,2}(0)} \quad (7)$$

Light intensity becomes:

$$I(\vec{s}) = [I_1(\vec{s}) + I_2(\vec{s})] [1 + \Re(\gamma_{1,2}(\tau))] \quad (8)$$

which, in the case of wave-fronts at infinity, as described in equation 2, and considering the on-screen coordinate x and the wavelength $\lambda = 2\pi c/\omega$, the light intensity becomes:

$$I(\vec{s}) = [I_1(\vec{s}) + I_2(\vec{s})] \left[1 + \mu \cos\left(\frac{2\pi x}{\lambda} + \phi\right) \right] \quad (9)$$

μ being the modulus of $\gamma_{1,2}(0)$ and ϕ its phase.

This co-sinusoidal modulation of the light is called an interferogram and is what one can measure using an interferometer (x is then modulated spatially - multiaxial instrument - or temporally - coaxial instrument - see Fig. 4).

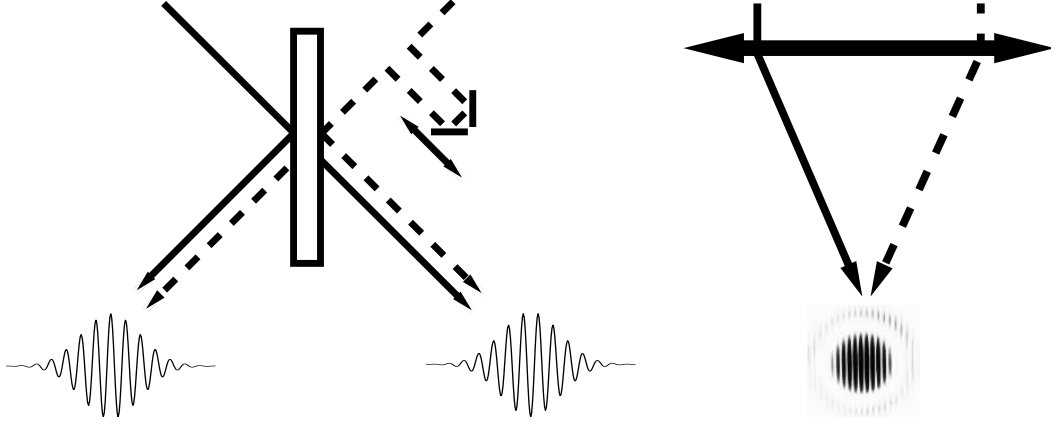


Fig. 4. Coaxial vs multi-axial beam recombination. In co-axial recombination, the fringes are scanned by a temporal modulation, whereas for multi-axial, the different pixels of the detector scans different OPDs. The nature of the recorded signal is then different and different biases affect them.

The Van-Cittert / Zernike theorem:

The Van-Cittert / Zernike theorem describes the relation between what we call the “complex visibility” (i.e. $\mu_{1,2} = \gamma_{1,2}(0)$) of an object and its brightness distribution $o(\vec{\alpha})$ on the plane of the sky. One can find its demonstration in various books, such as Goodman (1985).

Theorem: *For a non-coherent and almost monochromatic extended source, the complex visibility is the normalised Fourier transform (hereafter FT) of the brightness distribution of the source.*

By definition, the visibility μ is a complex number, whose modulus is between 0 and 1 (see Fig. 9 for an example in the case of a mono-pupil instrument). It is by definition:

$$\mu(\vec{u}) = \frac{\tilde{o}(\vec{u})}{\iint o(\vec{\alpha})} \quad (10)$$

where $\tilde{}$ represents the FT. By definition, when one measures $\|\mu\| < 1$, the object observed is *resolved* by the instrument. We can see here that interferometry does not provide direct access to the image of an object, as single-dish telescopes do. It is sensitive directly to the FT of the

brightness distribution of the object.

1.6 Practical considerations

Optical long-baseline interferometry has several intrinsic difficulties:

- (1) the intrinsic complexity to measure the data,
- (2) the apparent complexity for understanding the interferometric measures,
- (3) the very sparse sampling of data,
- (4) the relative bad sensitivity compared to single-dish experiments.

1.6.1 Measurement complexity

The first problem can be divided into two main problems:

- The atmospheric effect on ground-based observatories produces very fast and varying phase variations. In the case of single-dish telescopes, this effect typically reduces the angular resolution to the one of a telescope of the Fried diameter r_0 (Fried, 1965). Today, the advent of adaptive optics allows one to reach much higher angular resolutions at the cost of monitoring the atmosphere effects very fast and limiting the accessible magnitude. In the case of interferometry, long exposure times are not possible due to this atmospheric phenomenon. Therefore, just like with adaptive optics, a fast feedback loop must operate to correct the fringes motion. This is the only way of getting longer exposure times with the science instrument (see Fig. 5).
- The use of many subsystems in an interferometer (telescopes, delay lines, image sensors, fringe sensors, adaptive optics, focal instruments, etc.) can also be an issue. The more complex the interferometer gets, the higher the probability of failure. System optimisation is then a key point to manage these complex systems.

1.6.2 Interferometry understanding

The second problem is about to be solved with the development of general astrophysics instruments (AMBER is an example), and the preparation and interpretation of observations can be done with easy-to-use tools (developed

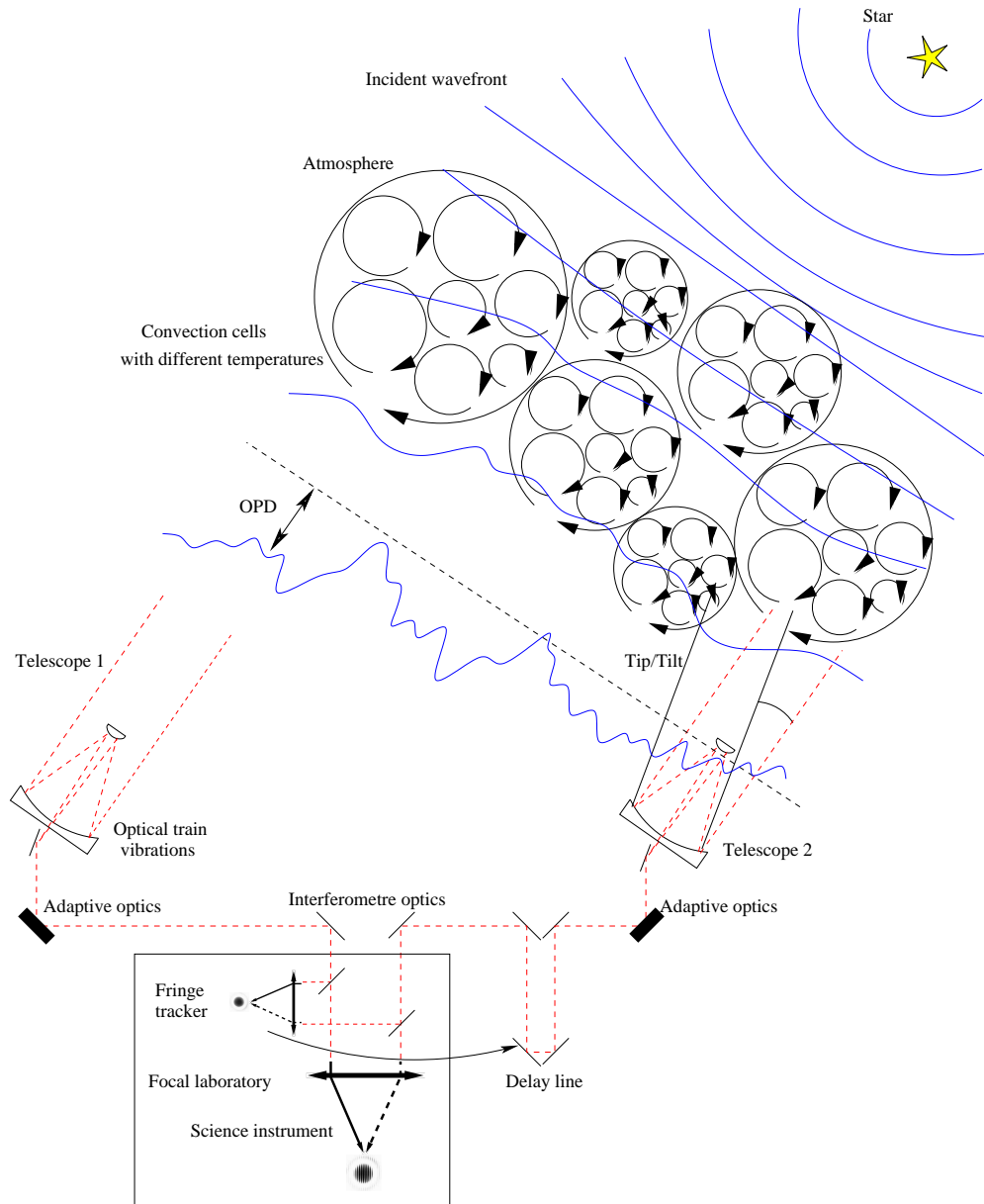


Fig. 5. This figure shows the main effects affecting an interferometric measurement: the atmospheric OPD being the most dominant by far. It also shows today's solutions to correct these effects: adaptive optics (or a tip/tilt correction for small apertures) for telescope effects, and fringe tracker and delay lines for interferometer effects.

by ESO¹, JMMC², and MSC³). For the general user, continuous trainings and summer schools are intended to help with the data interpretation.

¹ European Southern Observatory

² Jean-Marie Mariotti Centre

³ Michelson Science Centre

1.6.3 *Sparse sampling*

The third problem is also a 2-part problem:

- The limited number of telescopes (currently 3 on the VLTI, 4 with the second generation, 6 maximum for CHARA) generates a very sparse sampling of the (u,v) plane.
- The atmosphere makes it very difficult to access the object's phase and prevents a direct measurement of it. Several methods exist to partially retrieve the phase:
 - the phase closure (starting from 3 telescopes),
 - the differential phase (using a spectrograph),
 - the phase reference.

Today, the phase closure is the most widely used since it is easiest to calibrate.

The strategy to observe and interpret the data is then very different from what can be done with imaging facilities (such as single-dish telescopes, at a lower spatial resolution).

1.6.4 *Low sensitivity*

The last problem is also about to disappear with the advent of new generation interferometers like Keck-I or VLTI, combining long baselines and very large apertures.

2 (u,v) plane properties

As was seen in the previous section, an interferometer is sensitive to the FT of an object's brightness distribution. The question of Fourier plane (also called (u,v) plane) sampling is then crucial to know what part of the object's information the observer really observed. This section explains how to get a sufficiently good (u,v) coverage for an observation using a given interferometer.

2.1 *Super-synthesis*

The idea behind this word is to use Earth rotation to get a larger (u,v) sampling. Since a stellar interferometer baseline is fixed on the ground, its projection on the sky plane changes as the Earth rotates. This baseline projection depends only on the hour angle h (i.e. $h = \text{LST} - \text{R.A.}$), the baseline coordi-

ates (X, Y, Z) and the declination of the object δ . A change of coordinates links the baseline position and its projection on the plane of the sky:

$$\begin{pmatrix} u \\ v \\ w \end{pmatrix} = \frac{1}{\lambda} \begin{pmatrix} \sin(h) & \cos(h) & 0 \\ -\sin(\delta)\cos(h) & \sin(\delta)\cos(h) & \cos(\delta) \\ \cos(\delta)\cos(h) & -\cos(\delta)\sin(h) & \sin(\delta) \end{pmatrix} \begin{pmatrix} X \\ Y \\ Z \end{pmatrix} \quad (11)$$

The (u,v) coordinates for a given object (δ fixed) depend only on a linear expression of $\cos(h)$ and $\sin(h)$. These coordinates lies on an ellipse, as seen in Fig. 6. The time spent on the object will determine the increase in (u,v) coverage. However, the relation between the (u,v) filling and this time span cannot be intuitively estimated. Therefore, one has to check this for each studied case.

2.2 Number of telescopes

The relation between the number of telescopes combined and the number of baselines is the following (See Monnier , 2003):

$$N_b = \frac{N_t(N_t - 1)}{2} \quad (12)$$

The quantity measured is the amplitude and phase of the visibility function at the given baselines. Therefore, the total number of measurable information is:

$$N_m^{tot} = N_t(N_t - 1) \quad (13)$$

However, in optical long baseline stellar interferometry, things are not that simple. When using one spectral bin (for example, with a large band instrument) the phase information on each baseline is completely lost due to the atmosphere random phase noise insertion. However, some phase information can be retrieved with the phase closure when using 3 or more telescopes. The

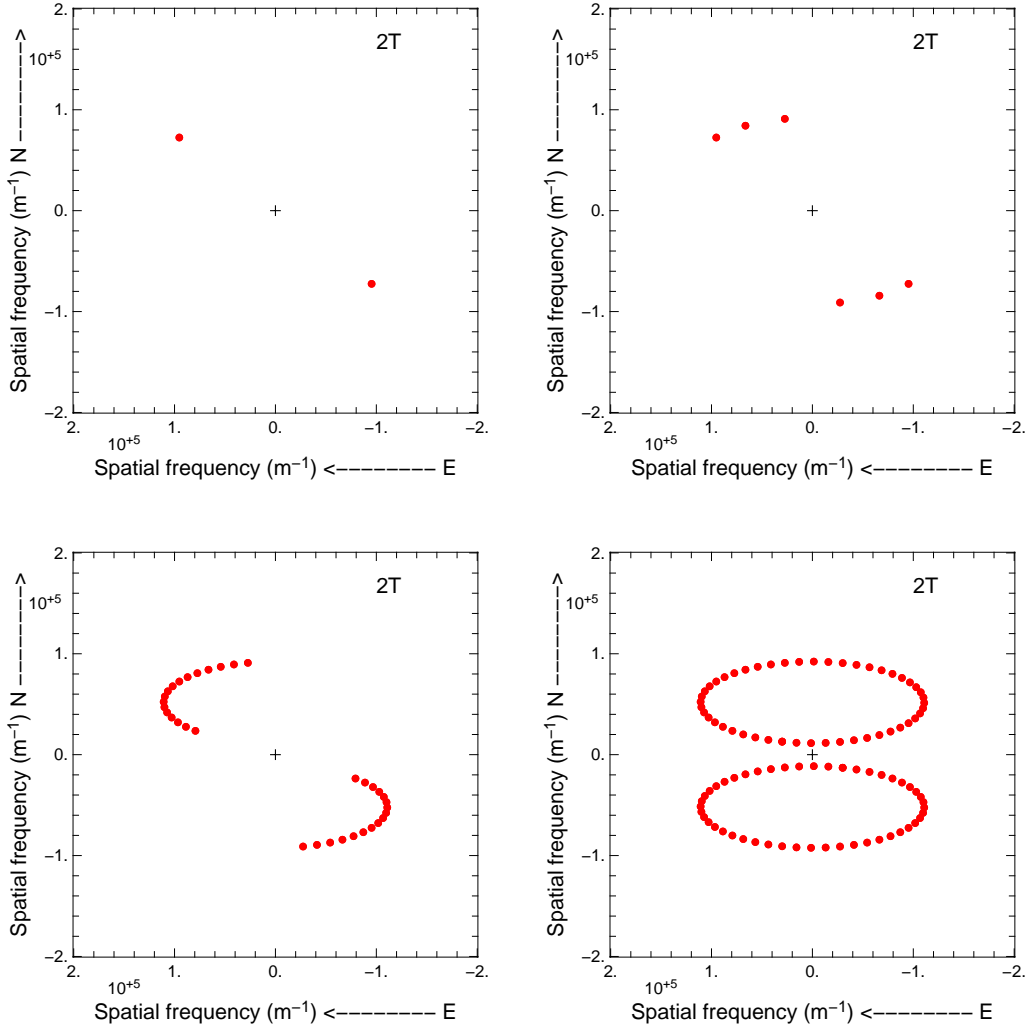


Fig. 6. Starting from a snapshot with 2 telescopes (UT1-UT4, top left), and increasing both the time sampling (1.5h top-right and 1/2h bottom-left) and the total integration time (1/2 night top-right and 1 night bottom-left), one can see that the (u,v) path is an arc of an ellipse (bottom-right).

number of phase closures measurable is:

$$N_c = \frac{(N_t - 1)(N_t - 2)}{2} \quad (14)$$

One normally has access to $\frac{N_t(N_t-1)}{2}$ amplitudes and $\frac{(N_t-1)(N_t-2)}{2}$ phases in interferometry. This gives the actual measurable number of information:

$$N_m^{act} = (N_t - 1)^2 \quad (15)$$

The comparison between eq.12 and 14 (see Fig. 7) and also between eq.13 and 15 suggest that the more telescopes you have, the better you can measure information at once.

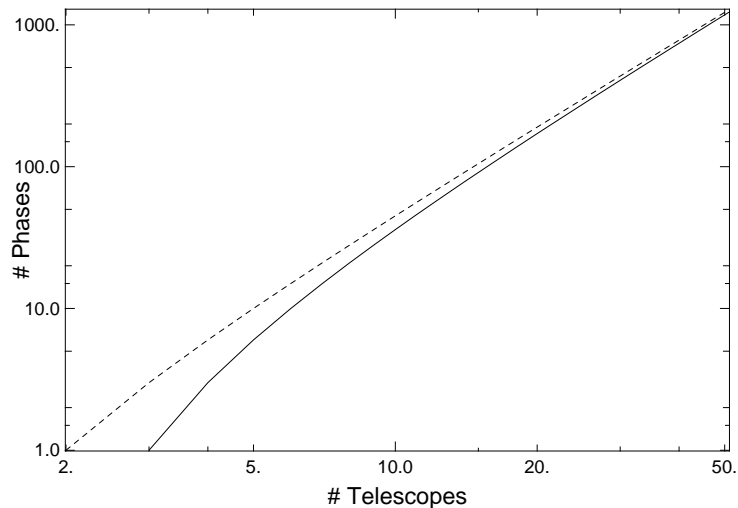


Fig. 7. One gain on 2 sides when adding telescopes to an optical long baseline stellar interferometer. The first is the squared increase of available baselines (dashed line). The second advantage is the phase closure information (full line) that grows faster for a few number of telescopes and tends to the maximum number of measurable phases (one per baseline, dashed line) for a high number of telescopes.

2.3 Spectral coverage

Spectral coverage helps in filling the (u,v) plane simply because different wavelengths probe different spatial frequencies for a given baseline:

$$\rho = \frac{B}{\lambda} \quad (16)$$

Thus, using a spectroscopic interferometer allows one to scan a line in the (u,v) plane with only one snapshot (see Fig. 8, top-right). The more spectral range an instrument has, the more (u,v) plane filling it gives.

Moreover, spectral coverage also allows one to greatly improve the number

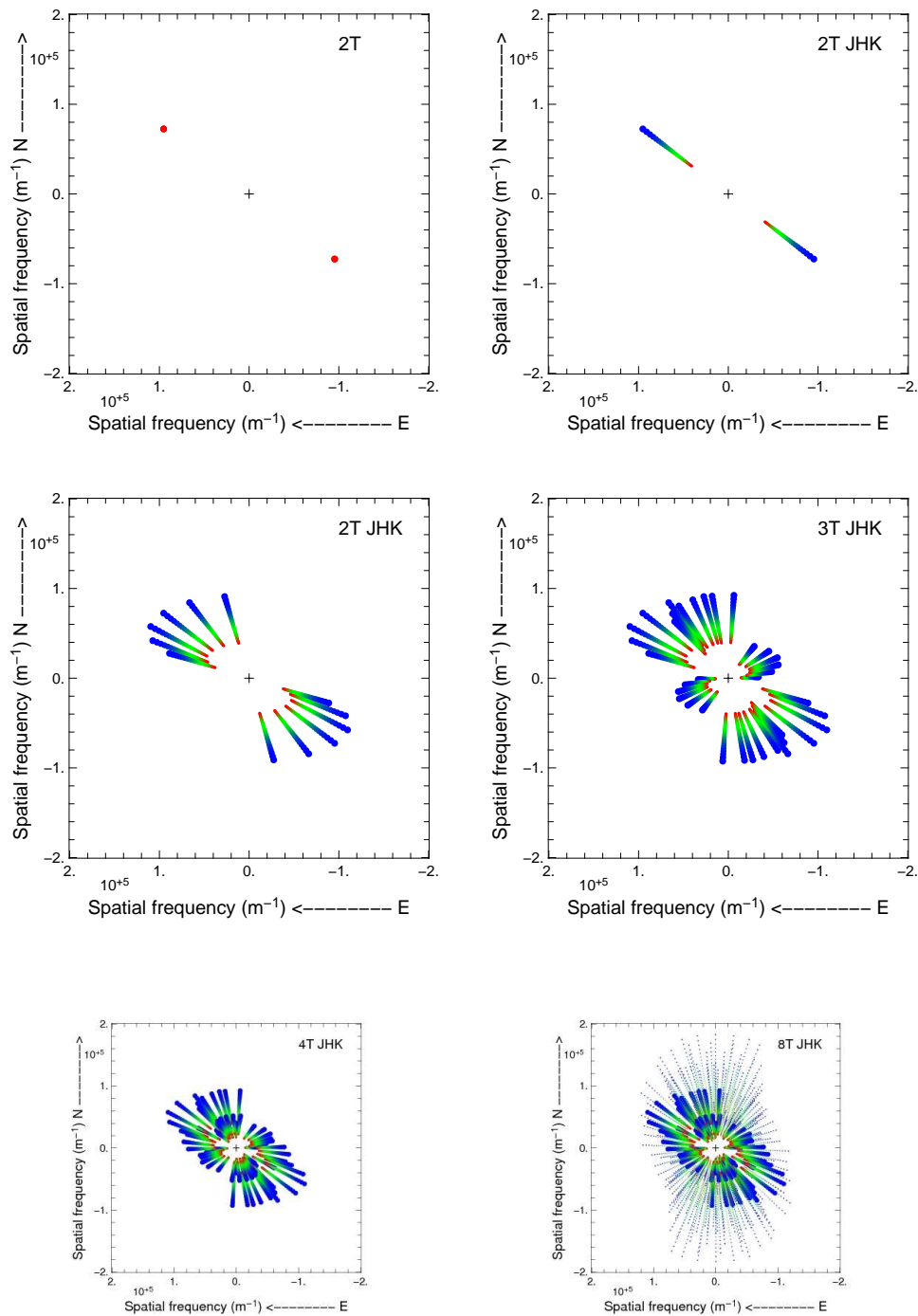


Fig. 8. **Top-left:** (u,v) coverage of a single snapshot with a single spectral bin instrument (ex: VINCI). **Top-right:** The same but using spectroscopic capability (ex: AMBER 2T). **Middle-left:** Adding super-synthesis to the last case improves (u,v) coverage. **Middle-right:** The same as before but using 3 telescopes (AMBER today). **Bottom-left:** Using 4 telescopes. **Bottom-right:** Using 8 telescopes (4 Afs, thin lines and 4 UTs, thick lines).

of measures one can access since more phase information is accessible via differential phase, as explained in detail in Millour (2006).

However, such improvement assumes that the object’s shape is achromatic with regards to wavelength. For example, in the specific case where the object’s shape is different for each wavelength, then this spectral coverage property does not improve (u,v) coverage.

As a matter of conclusion, combining many telescopes, a long observing time, and spectral coverage allows one to get a better (u,v) coverage of an object. Since the number of telescopes is very limited and many instruments were not able to spectrally analyse the light until recently, the only way was to increase the exposure time. Today, both the spectral coverage and the number of telescopes is increasing (6 telescopes for CHARA and simultaneous J, H and K bands for AMBER are examples), which allows one to begin imaging of the targets.

3 The shape-visibility relation

Here I add several notations to the previous ones:

- $r = \|\vec{s}\|$,
- $\rho = \|\vec{u}\|$,
- a, l, L are the object’s typical dimensions (diameter, FWHM, etc. if any),
- R is a flux ratio (if any).

As seen in previous sections, the measurement of an interferometer is related to the FT of the brightness distribution of the object. The goal of this section is to show the (complex) visibility description and to have some generic laws one can use to perform a simple interpretation.

3.1 Generic properties

First of all, one always has to have in mind that interferometry deals with FTs. We recall here the generic properties of FTs for continuous functions:

- **linearity (addition):** $FT[f + g] = FT[f] + FT[g]$,
- **translation (shift):** $FT[f(x - x_0, y - y_0)] = FT[f](u, v) \times e^{2i\pi \cdot (ux_0 + vy_0)}$,
- **similarity (zoom and shrink):** $FT[f(\alpha x, \beta y)] = \frac{1}{\alpha\beta} FT[f]\left(\frac{u}{\alpha}, \frac{v}{\beta}\right)$,
- **convolution (“blurring”):** $FT[f \otimes g] = FT[f] \times FT[g]$,
- **∞ limit (“small” details):** $FT[f] \xrightarrow{\infty} 0$,

- **0 limit (“large” details):** $FT[f] \xrightarrow{0} 1$.

The last two points lead to a specificity of optical long-baseline stellar interferometry: the best constraints for a model will be given by a measured visibility of 0.5. This translates into:

- For short baselines (i.e. small spatial frequencies), all the possible shapes have degenerate visibilities. The visibility modulus has a squared dependency with base length (see Fig. 10 and the demonstration in Lachaume , 2003) and its phase has a linear dependency.
- For long baselines, all continuous models (i.e., the ones not including δ functions) have visibilities towards 0. For a given accuracy on the measurements, therefore, no discrimination between different models can be done as the object is “over-resolved”.

Therefore, to maximise the efficiency of an observation, one has to know the approximate shape and size of an object in advance (1st guess). The knowledge of an object must then be as high as possible to maximise the chances of success of an interferometric observation. Once the observations have been made, and for a given model, there are many ways to fit the visibilities without changing the model itself:

- change the distance (using similarity),
- change the orientation in the plane of sky (using linearity and coordinate transformations),
- shrink or expand the model on one axis (using similarity), or
- blur the model (using convolution).

The two first points are useful for model fitting as one model image FT can be scaled and rotated to fit the observed data.

3.2 *Examples*

Here I present typical examples where the visibility function can be computed easily with an analytical formula. They are the basis of all further analysis, allowing one to get a first idea of the object’s shape without doing a complete physical modelling.

3.2.0.1 Point source: double or multiple star A centered point source is described in the Fourier plane by a constant. For many stars, even if the resolving power of interferometry is much higher than for single-dish telescopes, a good approximation of their shape can be made, assuming they are unre-

solved. The shift and add properties of the FT give the visibility expression for a multiple star:

$$V(\vec{u}) = \frac{\sum_{k=1}^N I_k \cos\left(\frac{\vec{u} \cdot \vec{s}_k}{\lambda}\right)}{\sum_{k=1}^N I_k} \quad (17)$$

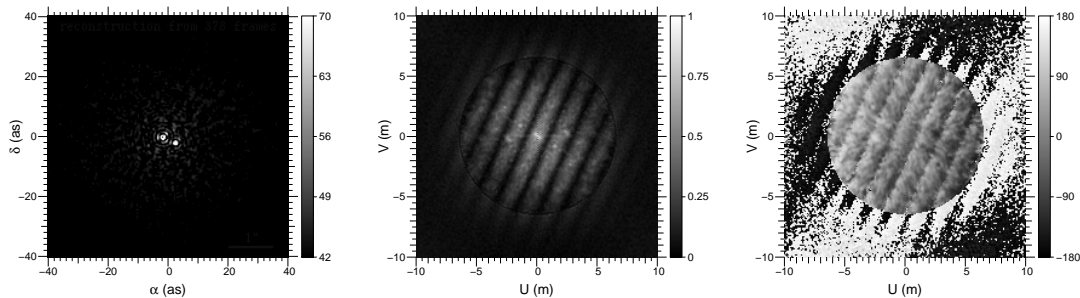


Fig. 9. Example (taken from Balega et al. , 2006) of a diffraction-limited image of a binary star (HIP 4849, observed at the Special Astronomical Observatory, Zelentchouk, left). The complex visibility of this image (middle and right) gives typical waves until the cut-off frequency of 6 m (features at larger frequencies are produced by the image reconstruction algorithm used here).

3.2.0.2 Gaussian disk: extended envelope In a first approximation, a Gaussian brightness distribution can describe several types of envelopes, such as an opaque wind surface around Wolf-Rayet stars, gaseous or dusty disks around young stars, etc. A Gaussian brightness distribution has a Gaussian visibility function:

$$V(\rho) = e^{-\frac{(\pi a \rho)^2}{4 \ln 2}} \quad (18)$$

3.2.0.3 Uniform disk: stellar surface In a first attempt, a uniform disk brightness distribution is well suited to describe a stellar surface, since, in general, the stars look like a sharp-edged disk, corresponding to the photosphere surface. The visibility function of a uniform disk is a 1st order Bessel function divided by $\pi a \rho$:

$$V(\rho) = \frac{J_1(\pi a \rho)}{\pi a \rho} \quad (19)$$

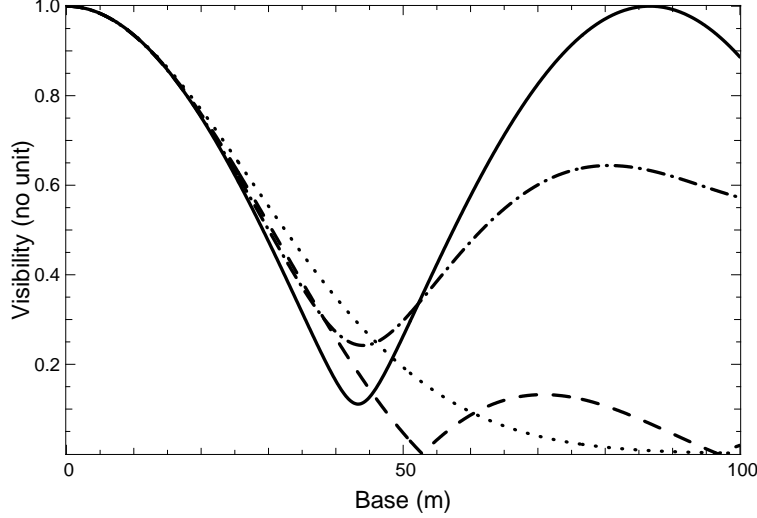


Fig. 10. Whichever model is used (binary star in solid line, Gaussian disk in dotted line, uniform disk in dashed line, or a composite object in dash-dotted line), the small baselines do not allow one to distinguish its shape.

3.2.0.4 Ring and Hankel function: any circular object A ring can describe a thin shell around a star. Its expression depends on the 0th order Bessel function:

$$V(\rho) = J_0(\pi a \rho) \quad (20)$$

It is also very interesting to use the addition property of the FT to produce the visibility function of any circular object with a given profile $I(r)$:

$$V(\rho) = 2\pi \int_0^\infty I(r) J_0(2\pi r \rho) r dr \quad (21)$$

3.2.0.5 Other objects For other objects, however, no simple tool except FT can be used. The best thing is to produce an image for the object in each wavelength of interest and then produce its FT and compare it with the visibilities.

In Table 2, one can see a summary of the different possibilities offered to test simple models.

Table 2

Summary table for simple shapes and their corresponding complex visibility.

Shape	Brightness distribution	Visibility
Point source	$\delta(\vec{s})$	1
Binary star	$A[\delta(\vec{s}) + R\delta(\vec{s} - \vec{s}_0)]$	$\sqrt{\frac{1+R^2+2R\cos\left(\frac{\vec{u}\cdot\vec{s}_0}{\lambda}\right)}{1+R^2}}$
Gauss	$I_0\sqrt{\frac{4\ln(2a)}{\pi}} \times e^{-4\ln 2\frac{r^2}{a^2}}$	$e^{-\frac{(\pi a \rho)^2}{4\ln 2}}$
Uniform disk	$\begin{cases} \frac{4}{\pi a^2} & \text{if } r < \frac{a}{2} \\ 0 & \text{otherwise} \end{cases}$	$\frac{J_1(\pi a \rho)}{\pi a \rho}$
Ring	$\frac{1}{\pi a} \delta\left(r - \frac{a}{2}\right)$	$J_0(\pi a \rho)$
Any circular object	$I(r)$	$2\pi \int_0^\infty I(r) J_0(2\pi r \rho) r dr$
Pixel (image brick)	$\begin{cases} \frac{1}{lL} & \text{if } x < l \text{ and } y < L \\ 0 & \text{otherwise} \end{cases}$	$\frac{\sin(\pi x l) \sin(\pi y L)}{\pi^2 x y l L}$

4 Conclusions

I have reported the main things to know about astronomical optical interferometry: a short history, the main principles, and the main properties of the measurements one gets from optical long baseline interferometry. Using this information, and by doing the practical exercises associated with this article, a future observer should be able to prepare observations knowing the real limitations but also the true possibilities of today's interferometers.

Acknowledgements

The author thank the Max-Planck Institut for Radioastronomy for support and funding through a stipend for the years 2007 and 2008. Thanks also to Gerhard Hühedpohl who allowed use of one of his aerial photos in the AMBER data reduction software. Part of this work and figures were made with the Yorick⁴ scientific software and amdlib⁵ AMBER data reduction software.

⁴ <http://yorick.sourceforge.net>

⁵ <http://amber.obs.ujf-grenoble.fr>, section data processing

References

- Thomas Young, Outlines of experiments and inquiries respecting sound and light London : Philosophical Transactions, 1800
- Fizeau, H., Sur un moyen de déduire les diamètres des étoiles de certains phénomènes d'interférence, 1851
- Stephan, E., C. R. Acad. Sci., 1874, 78, 1008
- Michelson, A.A. & Pease, F.G. Measurement of the diameter of alpha Orionis with the interferometer., 1921, 53, 249-259
- Pease, F.G., The Angular Diameter of a Bootis by the Interferometer, 1921, 33, 171
- Merrill, P.W. No. 240. Interferometer observations of double stars. Contributions from the Mount Wilson Observatory / Carnegie Institution of Washington, 1922, 240, 1-13
- Pease, F.G. Ergebn. Exacten Naturwiss., 1931, 10, 84-96
- Reber, G. & Greenstein, J.L. Radio-frequency investigations of astronomical interest The Observatory, 1947, 67, 15-26
- Ryle, M. A New Radio Interferometer and Its Application to the Observation of Weak Radio Stars Royal Society of London Proceedings Series A, 1952, 211, 351-375
- Smith, F.G. The Measurement of the Angular Diameter of Radio Stars Proceedings of the Physical Society B, 1952, 65, 971-980
- Butler, B.J.; McKinnon, M.M.; Perley, R.A. & Dewdney, P.E. The Expanded Very Large Array (EVLA) Astronomical Facilities of the Next Decade, 26th meeting of the IAU, Special Session 1, 16-17 August, 2006 in Prague, Czech Republic, SPS1, 18, 2006, 1
- Cohen, M.H.; Moffet, A.T.; Schilizzi, R.T. et al., J.D. Observations with a VLB array. I - Introduction and procedures , 1975, 201, 249-255
- Hanbury Brown, R. & Twiss, R.Q. A test of a new type of stellar interferometer on Sirius , 1956, 178, 1046
- Labeyrie, A. Interference fringes obtained on VEGA with two optical telescopes , 1975, 196, L71-L75
- Merkle, F. Concept of the ESO-VLT Project-Beam Combination Mitteilungen der Astronomischen Gesellschaft Hamburg, 1986, 67, 202
- Coudé du Foresto, V.; Perrin, G.; Mariotti, J. et al., The FLUOR/IOTA fiber stellar interferometer in *Integrated Optics for Astronomical Interferometry*, 1997, 115-125
- Perrin, G., The calibration of interferometric visibilities obtained with single-mode optical interferometers. Computation of error bars and correlations, A&A, 2003, 400, 1173-1181
- Perrin, G., Subtracting the photon noise bias from single-mode optical interferometer visibilities, A&A, 2003, 398, 385-390
- Goodman, J. W. Statistical optics New York: Wiley, 1985
- Fried, D. L. Optical Resolution Through a Randomly Inhomogeneous Medium for Very Long and Very Short Exposures Optical Society of America Jour-

- nal, 1966, 56, 1372-1379
- Monnier, J. D. Optical interferometry in astronomy. Reports of Progress in Physics, 2003, 66, 789-857
- Millour, F. Phd. thesis, Interférométrie différentielle avec AMBER, Université Joseph Fourier, 2006
- Lachaume, R. On marginally resolved objects in optical interferometry A&A, 2003, 400, 795-803
- Balega, I. I.; Balega, Y. Y.; Hofmann, K. et al. Orbits of new Hipparcos binaries. II, A&A, 2006, 448, 703-707